Tunable ultrafast control of plasmonic coupling to gold films

Nir Rotenberg,* Jan N. Caspers, and Henry M. van Driel
Department of Physics and Institute for Optical Sciences, University of Toronto, Toronto, Ontario, Canada M5S 1A7
(Received 15 September 2009; revised manuscript received 2 November 2009; published 15 December 2009)

We demonstrate ultrafast modulation of the coupling efficiency of free-space radiation to a surface plasmon polariton mode on a gold film with a PMMA grating overlayer over a broad range of wavelengths (540–700 nm). We observe modulation magnitudes of up to 14% at the center of the resonance, or 61% at the outlying regions. The limitations of this method are explored using simulations of the nonequilibrium electron thermal dynamics of the gold and of the response of the grating structure.

DOI: 10.1103/PhysRevB.80.245420 PACS number(s): 78.68.+m, 73.20.Mf, 78.20.Nv, 78.47.J−

I. INTRODUCTION

The ability to generate surface plasmon polaritons (SPPs), binding light to the surface of a metal, has fired the imagination of researchers worldwide and has opened new avenues toward the realization of nanophotonic devices.[1,2] One of the major challenges in this field is the ability to actively control—to switch or modulate—SPPs in such a device in a fast and efficient manner. In earlier work, active plasmonic elements such as extraordinary transmission-based switches[3,4] or plasmonic modulators based on phase transitions in semiconductor[5] or organic[6] films suffered from long switching times on the order of microseconds, too slow for modern information processing technologies, or were limited to the THz range. More recently, we and our colleagues demonstrated that the coupling resonance of free-space radiation to a SPP mode could be shifted on a sub-picosecond time scale due to ultrafast heating of free carriers by ultrashort laser pulses.[7] However, the deep gold gratings used in that study led to a spectral broadening of the SPP resonance, reducing the magnitude of the shift. Shortly thereafter, MacDonald *et al.*[8] demonstrated ultrafast modulation of propagating SPPs on aluminum films at 780 nm with a pulsewidth limited sub-picosecond component related to the excitation of a spectrally narrow interband resonance centered at 800 nm, and a 50 ps component related to the relaxation of hot electrons. However, both studies reported the peak modulations of the coupling efficiency to be smaller than 10%, making high-contrast applications difficult.

In this work, using a dielectric grating on a thin gold film, we provide a systematic study of the shifts and modulations of SPP resonances achievable due to electronic heating induced by intense 700 fs laser pulses. We characterize the response of our system both by varying the pump fluence, as well as by tuning the SPP resonance between 540 and 720 nm, showing peak modulations between 10% and 20% at the center of the resonance, and up to 60% off center while retaining sub-picosecond switching times. We then outline a method to model this type of plasmonic modulator. As an example, we employ this model for a gold grating and use the results to explore the boundaries of this approach to active plasmonic control.

This method offers a unique blend of advantages: not only is this the first broadband demonstration of such plasmonic modulation but also by careful selection of the excitation geometry it is possible to modulate each wavelength in either a negative or a positive fashion. Further, the thermalization dynamics of the electrons allow for both modulations at certain wavelengths without changing the excitation geometry.[9–13]

II. THEORETICAL BACKGROUND

Our approach to active SPP control, as shown conceptually in Fig. 1, has a passive as well as an active component. Passively, a dielectric grating overlayer couples light to a SPP at the gold-dielectric interface as determined by the optical properties of both materials, as well as the excitation geometry. Actively, an ultrashort pump pulse excites the free electrons in the metal and the subsequent nonequilibrium

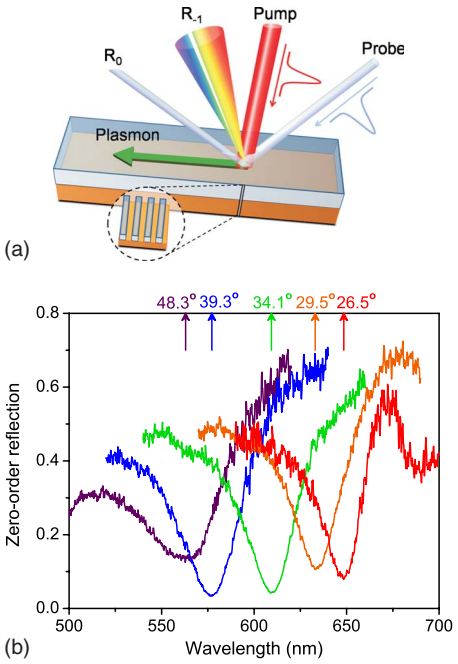

FIG. 1. (Color online) SPP excitation and modulation geometry. (a) A dielectric grating couples a broadband probe pulse to a SPP on a thin gold film. Transient thermal effects induced by a pump pulse modulate the coupling efficiency on sub-picosecond times. (b) Zero-order reflectivity spectra for *p*-polarized probe pulses incident at different incidence angles (top axis) show different SPP resonances.

thermalization dynamics lead to sub-picosecond modulation of the optical constants of the metal, and hence to sub-picosecond control of the SPP coupling.

A. Grating coupling of SPPs

A SPP, the propagating mode of oscillating surface electrons coupled to the oscillations of an electromagnetic wave, can be described by the following wave vector:[14]

$$k_{\mathrm{SPP}} = k_0 \sqrt{\frac{\varepsilon_d \varepsilon_m}{\varepsilon_d + \varepsilon_m}}, \tag{1}$$

where $k_0 = 2\pi/\lambda$ is the vacuum wave vector for light of wavelength λ and $\varepsilon_{m(d)}$ is the complex dielectric function of the metal (dielectric). Since $\varepsilon_m < 0$ it follows that $k_{\mathrm{SPP}} > k_0$ which ensures that the SPP remains bound to the surface of the metal and cannot simply reradiate once it is launched. Conversely, this momentum mismatch must be overcome to couple free-space radiation to a SPP mode.

One way to generate the required momentum is with a grating, as shown in Fig. 1(a), where the phase-matching condition becomes

$$k_{\mathrm{SPP}} = k_0 \sin\theta + mK_G, \tag{2}$$

where $k_0 \sin\theta$ is the component of the free-space momentum in the plane of the grating, $K_G = 2\pi/\Lambda$ is the wave vector of a grating of period Λ, and m is an integer. From this equation it is evident that the properties of a SPP resonance are, through k_{SPP}, very sensitive to the dielectric function of both bounding layers, as well as to the grating geometry. As predicted by Eq. (2), it is possible to systematically move the SPP resonance by changing the angle of incidence, θ, in this system [Fig. 1(b)].

B. Nonequilibrium thermal dynamics

To induce a change to the dielectric function of a metal we irradiate its surface with an ultrashort pump pulse, transferring energy to the free electrons through the absorption of the incident photons.[10] Although the electrons are initially in a nonthermal distribution,[11,12] electron-electron collisions establish a temperature within ~500 fs, after which the electrons can be described by Fermi statistics. Subsequently, electron-phonon collisions transfer energy from the electrons to the lattice, leading to a thermal equilibrium of the entire system in several picoseconds. This process can be described by the following system of coupled equations:[11]

$$\frac{\partial N}{\partial t} = -\frac{N}{\tau_1} - \frac{N}{\tau_2} + P(z,t),$$

$$C_e \frac{\partial T_e}{\partial t} = \frac{\partial}{\partial z}\left(K_e \frac{\partial T_e}{\partial z}\right) - g(T_e - T_\ell) + \frac{N}{\tau_1},$$

$$C_\ell \frac{\partial T_\ell}{\partial t} = g(T_e - T_\ell) + \frac{N}{\tau_2}, \tag{3}$$

where

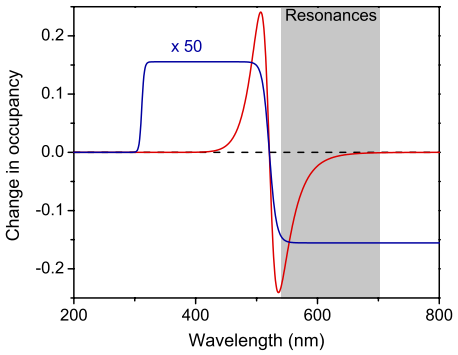

FIG. 2. (Color online) Change in occupancy of electronic states in gold for $T_e = 945$ K. Both the initial nonthermal (blue, 50× magnification) and the subsequent thermal (red) distributions, as well as the spectral region containing the plasmonic resonances (shaded) are shown.

$$P(z,t) = (1 - R_0)\alpha e^{-\alpha z} I(t)$$

is the power density absorbed, as a function of time, t, and depth, z, into the sample, from the incident beam with a temporal intensity profile $I(t) = I_0 \exp[-4(\ln 2)t^2/\tau_p^2]$ given a peak intensity I_0 and a full width at half maximum (FWHM) pulse length τ_p, coefficient of reflection R_0, and coefficient of extinction α. In the above, N is the nonthermal energy density, $T_{e(\ell)}$ is the electron (lattice) temperature, $\tau_1 = 0.5$ ps and $\tau_2 = 1.0$ ps are the electron and lattice thermalization times, respectively,[11] $C_{e(\ell)}$ is the electron (lattice) heat capacity, K_e is the thermal conductivity of the electrons, and g is the electron-phonon coupling constant. For our system, other than $\tau_{1(2)}$, the relevant parameters can be found in Ref. 15, though the extinction coefficient needs to be adjusted for an increased penetration depth of 100 nm due to the ballistic nature of the excited electrons.[16]

By solving the above equations we obtain the time dependence of N and T_e, each of which contributes to the change in the carrier distribution in the conduction band. We show these in Fig. 2 for irradiation with a 700 fs, 775 nm, and 80 mJ cm^{-2} pump pulse which results in a peak electron temperature of 945 K. For gold, the change in occupancy is centered about the d-band transition resonance, located near the Brillouin zone L point corresponding to a wavelength of 520 nm. It is interesting to note that during the early part of overlap, as energy is transferred from the pump pulse to the electrons, the change to the distribution function is mainly governed by the photon energy and intensity of the pump beam. Consequently, the broadband nature of the nonthermal distribution allows for sub-picosecond modulation of the dielectric function over an energy range well beyond what is possible due to thermal effects;[12] for example, for a pump pulse centered at 775 nm as used in this study, the effects of the thermal distribution extend from 400 to 650 nm, while the impact of the nonthermal distribution range from 300 nm and beyond 1500 nm.

The change in occupancy leads to a change in the imaginary part of the dielectric constant.[9] The Kramers-Kronig relation is then used to calculate the corresponding change to the real part. This procedure, then, yields the transient

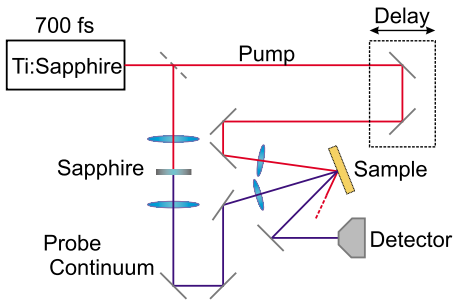

FIG. 3. (Color online) Schematic of the experiment.

changes to the frequency-dependent dielectric function of gold due to irradiation by ultrashort pump pulses.

In the spectral region where we demonstrate the operation of the SPP modulator, with photon energies below 2.38 eV (520 nm), the change to the optical properties can be understood as follows: the pump pulse excites electrons from previously filled electronic states in the conduction band to those above the Fermi level. Subsequently, the greater number of possible transitions cause the probe pulse to sense a positive change to the imaginary part of the dielectric constant, and a corresponding change to the real component. Since the coupling properties of light to a SPP are intimately dependent on the dielectric constant of the metal [Eqs. (1) and (2)], the probe pulse experiences a modulation of its coupling efficiency.

III. EXPERIMENTAL RESULTS AND DISCUSSION

We excite SPPs on a thin gold film with a polymethyl methacrylate (PMMA) grating overlayer. This is fabricated using the following procedure. First, we evaporate 200 nm of gold onto a silicon (100) wafer, with a 20 nm intermediate layer of Chromium for adhesion. We then spin 200 nm of PMMA onto the gold, into which we expose a 820 nm period grating via e-beam lithography, which we then develop. We ensure that resultant grating has a square profile with a period of 820 nm and an amplitude of 200 nm with a scanning electron microscope.

The transient experiments were performed using a pump-probe setup (Fig. 3). First, we couple a 700 fs (FWHM) broadband (450–750 nm) continuum (140 μm FWHM) to a gold film using a 820 nm period PMMA grating at different excitation geometries. The continuum is generated by focusing ~5 mW of light, from a 1 kHz Ti:sapphire laser amplifier operating at 775 nm, onto a sapphire window. Once a plasmonic resonance is identified for p-polarized light, we modulate the SPP coupling by pumping the gold film with the remainder of the 775 nm light (570 μm FWHM) which does not interact with the PMMA but induces a transient nonequilibrium carrier population in the gold as described in the previous section.

A. Sub-picosecond control of plasmonic coupling

We monitor the change to the coupling efficiency by varying the time delay between the pump and the probe and recording the zero-order reflectivity spectra (Fig. 4). Here the

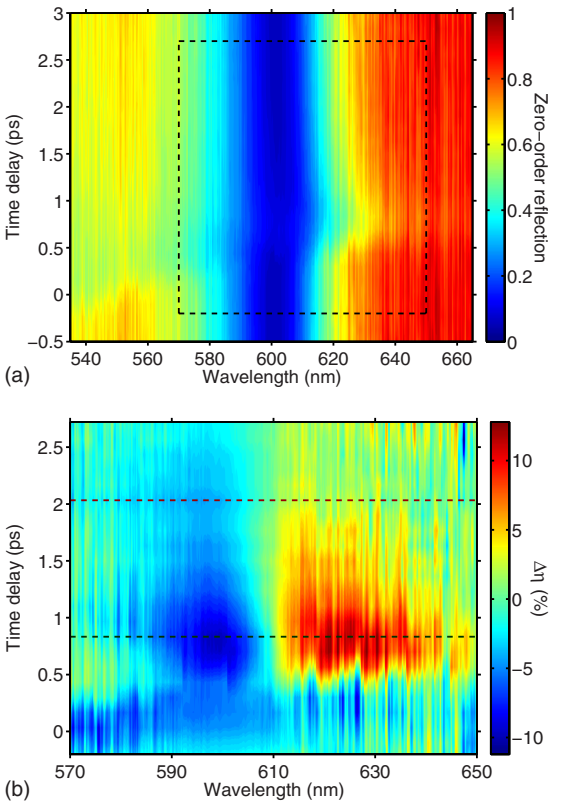

FIG. 4. (Color online) Ultrafast modulation of a single plasmonic resonance. (a) Zero-order reflectivity spectra as a function of time delay between pump and probe. The region of interest is bounded and shown in (b) as the change in the percentage of the initial probe light couples to a SPP, again as a function of time and wavelength.

reflectance is given as a function of both delay time and wavelength [Fig. 4(a)]. The plasmonic resonance is seen as a large dip centered at 603 nm. By considering the magnitude of the dip relative to the spectra before the pump arrives, we can extract the transient change to the coupling efficiency from the zero-order reflection as a function of both the delay time and the wavelength [Fig. 4(b)]. For clarity, this change is also given at fixed delay times as a function of wavelength [Fig. 5(a)] and at fixed wavelengths as a function of time [Fig. 5(b)].

Considering the ambient reflectivity of ~75% in the region of the resonance [Fig. 4(a)], we extract a SPP coupling efficiency of ~70% near the center of the resonance at 603 nm. At this wavelength, at the peak of the pump induced changes at 0.8 ps [lower dashed line in Fig. 4(b)] ~10% less light is coupled to a SPP mode, resulting in a coupling efficiency of ~60%. We define the pump-induced modulation to the coupling efficiency as

$$M(t) = \frac{\Delta\eta}{\eta_0} = \frac{\eta(t) - \eta_0}{\eta_0}, \tag{4}$$

where η_0 and $\eta(t)$ are the SPP coupling efficiencies before the pump pulse arrives and at time t, respectively (Fig. 6). The above situation results in a peak modulation of M_{max}= −14%. However, there exists a balance between the magni-

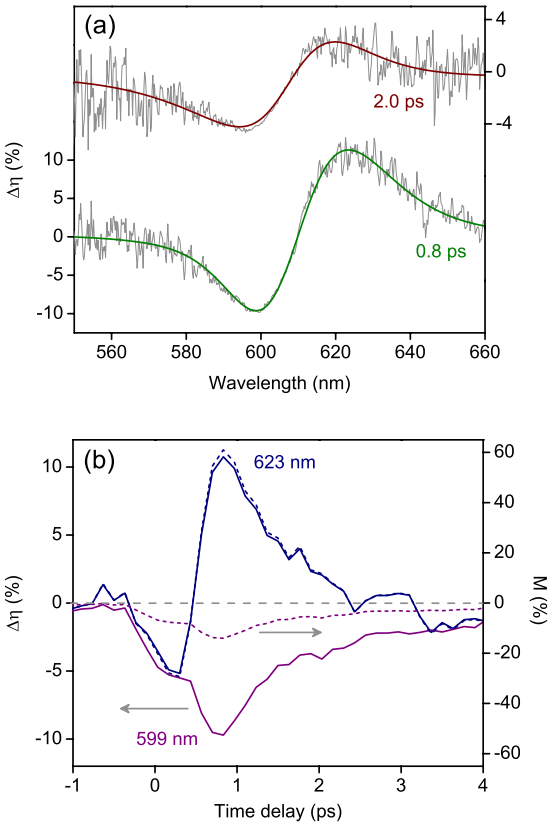

FIG. 5. (Color online) (a) Wavelength-dependent changes to the SPP coupling at peak (0.8 ps) and long (2.0 ps) delay times. (b) Transient changes (and modulation—dotted line, right axis) of the SPP coupling efficiency at 599 and 623 nm.

tude of the coupling efficiency achievable, and that of the peak modulation. Considering the cross-section of the peak changes in coupling efficiencies [Fig. 5(a)] we see that, near 623 nm, there is a 10% increase in the coupling efficiency. As this spectral region is further away from the center of the resonance, less light (η_0=16%) is initially coupled to a SPP

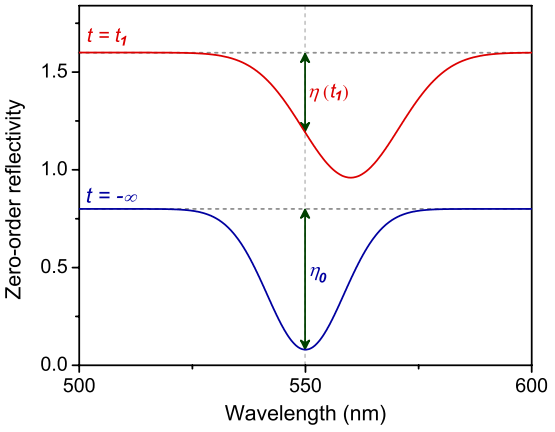

FIG. 6. (Color online) Explanation of the coupling efficiencies. We show two zero-order reflectivity spectra, vertically shifted for convenience, representing the initial ($t=-\infty$) and pumped ($t=t_1$) situations along with their respective coupling efficiencies at 550 nm, η_0 and $\eta(t_1)$.

mode. Consequently, at the peak of the changes, $\eta_{max} \approx 26\%$ leading to $M_{max}=61\%$. That is, the peak modulation can be increased at the cost of the absolute coupling efficiency and vice versa. We attribute the asymmetry in the location of the peak-coupling efficiency changes, relative to the center of the resonance, to the fact that both the real and imaginary parts of the dielectric constant are changed during the pumping process. Consequently, as a closer examination of Fig. 4(a) reveals, not only does the resonance shift but it also broadens, resulting in a redshift of the $\Delta\eta$, or M_{max}, spectra.

The sign of the modulation of any given spectral component depends on whether it is located on the long- or short-wave side of the SPP resonance. As we show in the following section, the $\Delta\eta$ spectra of a resonance centered above 560 nm redshifts, resulting in positive modulations on the long-wave side and negative for shorter wavelengths. Conversely, below 560 nm the SPP resonance blueshifts and the regions of positive and negative modulations reverse. We attribute this to the different slope of the induced change in the real component of the dielectric constant at different wavelengths; at wavelengths shorter than 560 nm it is negative, while for longer wavelengths it is positive, and, recalling Eq. (2), this leads to resonances in the two spectral regions shifting in opposite directions. Consequently, with careful consideration of the excitation geometry, a positive or negative modulation can be induced at any wavelength. As discussed above, the different times and processes by which the electrons and the lattice reach thermal equilibrium[11] have an intriguing effect. It is often possible to first modulate the SPP coupling with one sign and then, within a few hundred femtoseconds, to reverse the sign [Fig. 5(b)].

From these results and in particular from Fig. 5(b), we extract the time scales associated with this switching. The peak modulation to the coupling efficiency occurs about 800 fs after temporal overlap, when most of the pump-pulse energy has been transferred to the electrons in the metal and before it can be dissipated to the lattice or spread due to diffusion. Given our pulse lengths, this peak time is consistent with accepted thermal models.[10,11] By fitting an exponential decay to these curves, taking account pump and probe convolution effects, we extract a time constant of about 770 ± 70 fs which is consistent with earlier observations.[13]

B. Fluence and wavelength dependence

To characterize this method of SPP modulation we repeat these measurements, as outlined above, for different pump fluences [Fig. 7(a)], holding the initial resonance at 603 nm, and for different resonances [Fig. 7(b)]. The peak modulation, M_{max}, increases in a nonlinear fashion as a function of the pump fluence, to a peak value of about 60% for pump fluences of 60 mJ cm^{-2} [Fig. 7(a)]. This is both expected, as the thermal dynamics of the carriers are highly nonlinear,[11] as well as confirmed by earlier studies.[13] We find that the sample degrades at fluences >75 mJ cm^{-2}, related to multiphoton absorption induced damage to the PMMA grating.[17] At this threshold, we have observed modulation of almost

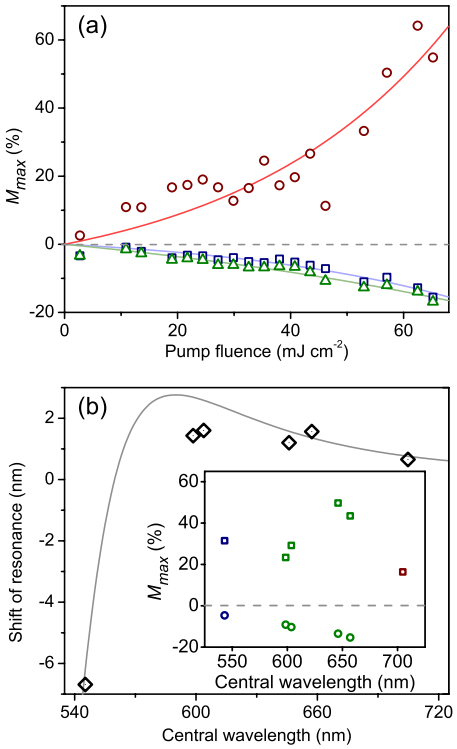

FIG. 7. (Color online) Characterization of modulation and shift of SPP resonances. (a) Peak modulations as a function of pump fluence for a SPP resonance at 603 nm. Shown are the peak positive (red circles) and negative (green triangles), as well as the modulation at the center of the plasmonic resonance (blue squares). The guide lines are exponential fits. (b) The peak shifts of the SPP resonance, as function of the original center of the resonance. The gray curve is proportional to the slope of the induced change to the real part of the dielectric function. The inset shows the peak positive and negative modulations achievable for different resonances. Pump fluences are: 45 mJ cm^{-2} at 540 nm, 50 mJ cm^{-2} between 600 and 650 nm, and 55 mJ cm^{-2} at 700 nm.

100% for wavelengths between 540 and 560 nm. We suggest that this modulation can be recovered, and the damage to the grating can be avoided either by moving to metallic gratings or by increasing the length of the pump pulse. The latter solution, in particular, is attractive since previous studies show that increasing the pulse length leads to an increase in the effective nonlinear changes to the optical properties of the metal.[13] Using the former approach, as we have done in our earlier study,[7] results in a more robust structure but complicates the fabrication process.

We demonstrate that modulation of SPP coupling can be achieved across a broad range of wavelengths by studying the shifts for plasmonic resonances at different wavelengths, holding the pump fluence constant at ~50 mJ cm^{-2} [Fig. 7(b)]. As expected [Eq. (1) and (2)], the peak shifts to the center of the resonances follow the relative changes to the real part of the dielectric constant in the spectral region considered. More interesting, we observe high modulations, in excess of 20%, for all visible wavelengths above 540 nm and only slightly smaller changes for wavelengths as long as 700 nm. As noted earlier, the peak modulation depends nonlinearly on the pump fluence, suggesting that

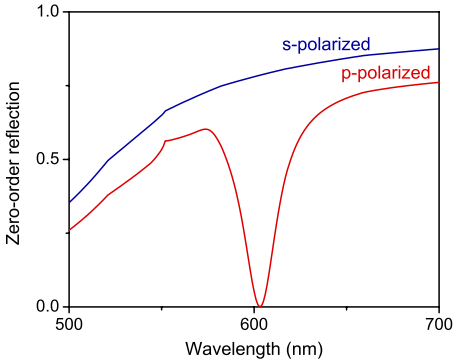

FIG. 8. (Color online) Theoretically calculated *s*- and *p*-polarized zero-order reflectances for a sinusoidal gold grating with an 820 nm period and 80 nm amplitude, keeping the angle of incidence fixed at 19°.

modulation in excess of 50% is possible for this entire region.

IV. SIMULATIONS

In the previous sections we have demonstrated that active control of plasmonic coupling can be achieved with a dielectric grating on top of a gold film. In earlier work, we showed that this type of control is also possible for gold gratings and that the modulation is due to the optically induced transient thermal dynamics of the electrons in the metal.[7] In what follows we present a procedure that can be used to fully model the response of these plasmonic couplers. Since the underlying physical process causing the modulation for both types of gratings is the same we focus our simulations on the gold grating. We would expect to recover good qualitative agreement for both types of experiments, and it is only the quantitative details which will change for each different application.

To explore the limits of the thermally induced modulation of the plasmonic coupling we simulate the response of the grating coupler using the numerical C Method, as described by Li *et al.*[18] Briefly, the chief challenge of modeling the diffraction from a grating lies in the nonplanar interface for which there are no analytic solutions for the electromagnetic fields that satisfy the boundary conditions. By transforming the coordinate system of the problem such that the grating profile becomes flat we ensure continuity of the electromagnetic radiation across the interface, though the fields must also be transformed appropriately. This approach results in a system of linear equations which we solve numerically to obtain the diffracted orders (both in reflection and in transmission) for the grating.

We repeat the calculation, keeping the grating geometry—sinusoidal gold grating with an 820 nm period and an 80 nm amplitude—with θ=19° kept constant, but varying the wavelength to build the expected reflection spectra (Fig. 8). For these calculation we use the complex dielectric function given in Ref. 19. We can immediately identify the SPP resonance by the sharp dip in the *p*-polarized spectra, in contrast with the featureless *s*-polarized spectra. Like the experimental spectra [cf. Fig. 4(a)], the location of the simulated reso-

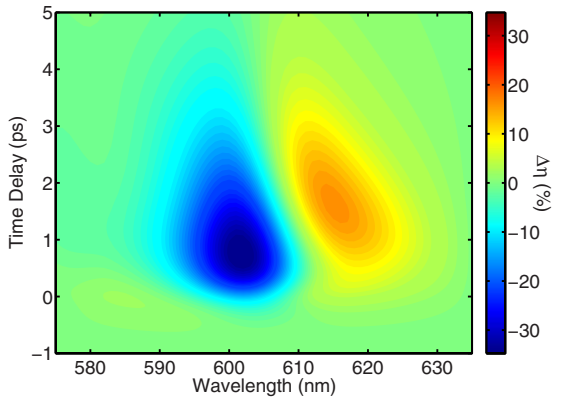

FIG. 9. (Color online) Change in coupling efficiency for an 80 mJ cm^{-2} pump as a function of wavelength and time.

nances is in good agreement with the theoretical predictions [Eq. (2)]. While the shape of the simulated spectra is the same as in the experiments, we note the SPP resonance predicted by this theory is sharper than what we have previously observed: we predict a FWHM of ~25 nm but observe a FWHM of ~35 nm. We attribute this difference to the following: (1) here we simulate a gold grating as opposed to the PMMA grating on top of a gold film which was used in the experiment. As noted in the previous section, by selecting a pure gold grating we are able to pump the system harder, and can therefore better test the limitations of this scheme. Since the penetration depth of the SPP into the dielectric is different than into the metal,[14] we can recover the absolute coupling efficiency in this new case by adjusting the amplitude of the grating. (2) These simulations implicitly assume a continuous plane wave, whereas we tightly focus Gaussian pulses onto the gratings. In particular, the limited spatial extent of our pulse can be thought of as introducing additional Fourier components to the grating profile, leading to a spectral broadening.

Using the same pump-pulse parameters, and following the procedure outlined in Sec. II B, we model the optical properties of the gold grating as a function of time and wavelength, and consequently we extract a reflection spectra for each time step. From these we calculate $\Delta\eta$; we show these results for an 80 mJ cm^{-2} pump (Fig. 9), the highest fluence that did not damage the gold. Qualitatively, this figure is in good agreement with the experimental results [Fig. 4(b)], though there are some quantitative differences. These fall under two categories: differences in the shape of the differential spectra and differences in its magnitude.

To facilitate the interpretations of these results we present various cross-sections in Fig. 10. We see the effects of the two different pump-induced changes to the optical properties most clearly by examining the location of the SPP resonance as we vary the delay time between the pump and probe pulses [Fig. 10(a)]. The initial nonthermal effects pull the resonance toward shorter wavelengths until the thermal effects can compensate and, eventually, dominate and shift the resonance toward the longer wavelengths. As one centers the SPP resonance at longer wavelengths, further away from the *d*-band transition resonance, the thermal effects weaken and the initial blueshift will increase, and the subsequent redshift decrease.

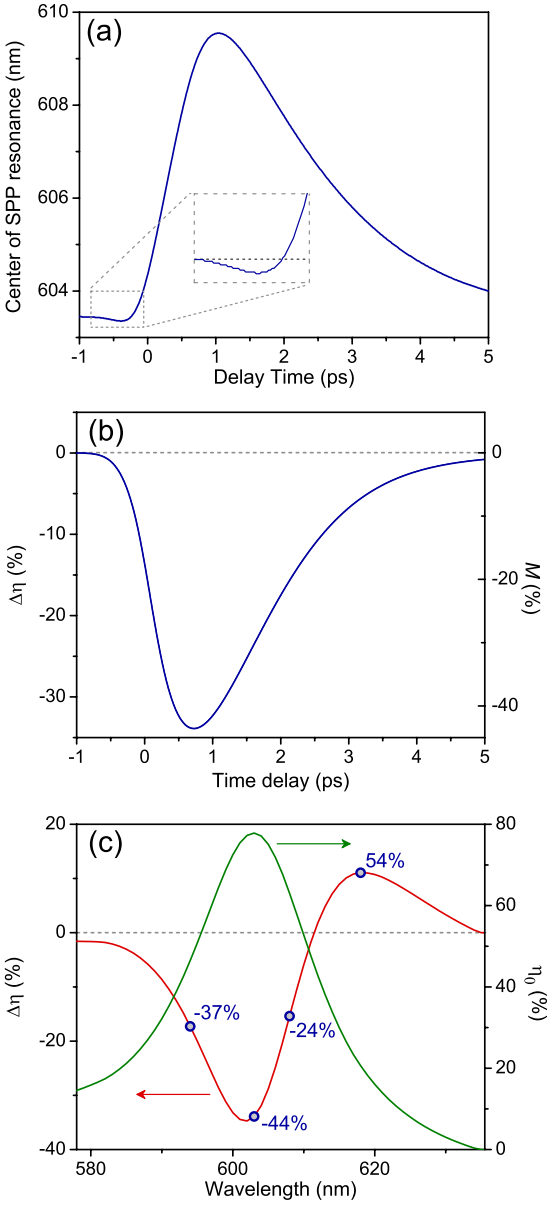

FIG. 10. (Color online) Results extracted from the full time wavelength-coupling efficiency simulations for a pump fluence of 80 mJ cm^{-2}. (a) The location of the center of the SPP resonance as a function of the time delay between the pump and probe pulses. (b) The time-dependent changes, $\Delta\eta$ (left axis), and modulation, M, (right axis) of the coupling efficiency at the center of the SPP resonance (603 nm). (c) The initial (right axis), η_0, and change (left axis), $\Delta\eta$, of the coupling efficiency as a function of wavelength at a delay time of 0.8 ps. At selected wavelengths, the modulation, M, is shown (circles).

By considering the transient changes to the coupling efficiency [Fig. 10(b)], we see that the time scales in the simulations match those in the experiments: the peak changes occur 0.8 ps after overlap, and the system recovers in ~1 ps. The marginally longer recovery time is due to the simplicity of the model, wherein we assume a perfect sample and limit the electronic energy loss to heat transfer with the lattice. It is interesting that, for all delay times, the modulation to the coupling efficiency is negative, in contrast with the shift of

the center of the resonance [Fig. 10(a)]. This hints at the complexity of the dynamics of the system: even as the resonance shifts, it also broadens, so that when it is passes through its original position the coupling efficiency is lower at the center, but higher for some outlaying regions.

We show the spectra of the changes to the coupling efficiency at a delay time of 0.8 ps, corresponding to the greatest changes at the center of the resonance [Fig. 10(c)], including the initial coupling efficiency for completeness. This figure shows good agreement with the experimental results [Fig. 5(a)], in that the short wavelength side of the resonance experiences a negative change, while to the long-wave side additional light is coupled to the SPP due to pumping. However, the changes occur in a narrower range than experimentally observed, a direct consequence of the narrower resonance.

Furthermore, unlike the experimental changes, the magnitude of the negative changes is larger than that of the positive changes. As discussed above, we attribute this difference to the assumptions inherent in this numerical method, the result of which is that the shift of the resonance dominates over the broadening. This nicely demonstrates the advantages of a narrower resonance and leads us to suggest that, for the practical applications of this method, the gratings used should be optimized to provide the narrowest possible SPP resonance.

Another consequence of this feature is that while the changes at the center of the resonance are greatly increased, those at the outlying regions are only slightly decreased. As a reference, we provide the corresponding modulations at several points along the $\Delta\eta$ spectra [Fig. 10(c), circles]. At the center of the resonance at 603 nm, where initially 77% of the light is coupled to the SPP, there is a peak-induced change of −34%, corresponding to a coupling efficiency of 43% or a peak modulation of −44%. At the same time, near 618 nm, there is a peak change to the coupling efficiency of 11%, corresponding to a modulation of 54%. As a comparison, recall the peak experimental modulations of −14% and 61% at the center and outlaying regions, respectively.

There are two more reasons that help account for the increase in the coupling efficiency at the center of the resonance. (1) The simulations employ a pump fluence of ~80 mJ cm^{-2} while the peak experimental values are for a fluence of ~60 mJ cm^{-2}, as a pure gold grating has a higher damage threshold than does one made out of PMMA. (2) When calculating the changes to the optical properties of the gold (cf. Sec. II B) we assume that the entire probe spot is pumped by the fluence given. Though the probe size (140 μm) is much smaller than that of the pump (570 μm) this assumption still introduces some error.

As both the relationship of the pump fluence to the change to dielectric function of the gold, as well as the value of the dielectric function to the response of the grating are highly nonlinear, they cannot be accounted for before the simulations. Consequently, we calculate $\Delta\eta$ and M for different pump fluences, summarizing the results in Fig. 11 for comparison with the experimental power study [Fig. 7(a)]. By interpolating between the points, we calculate an expected peak modulation of −31%, at the center of the resonance at a pump fluence of 60 mJ cm^{-2}. We correct this value by taking a weighted average of the pump fluence experienced by the probe due to its Gaussian profile and arrive at a peak modulation of −28%, a factor of 2 greater than experimentally observed. Near a pump fluence of 80 mJ cm^{-2}, the maximum fluence, the corrected modulation at the center of the resonance is −41%; even if nonideal conditions (e.g., focused beam instead of plane wave) introduce a factor of 2, this still sets a lower bound on the achievable modulation, at the wavelength of initial peak coupling efficiency, of −20%.

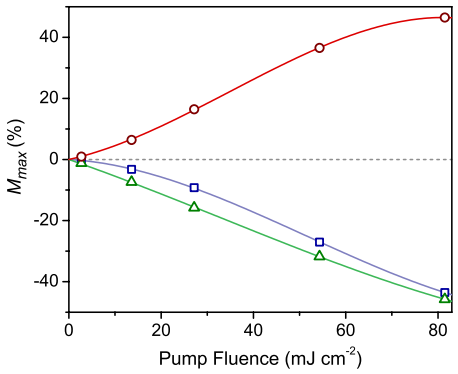

FIG. 11. (Color online) Power study of the simulations. For each pump fluence we show the peak achievable positive (circles) and negative (triangles) modulations, as well as the greatest modulation at the center of the SPP resonance (squares). The lines are guides for the eyes.

V. CONCLUSION

To summarize, we present a systematic study of an active plasmonic coupler based on ultrafast, optically induced thermal effects in a gold film with a grating overlayer. We demonstrate the method experimentally and outline a theoretical model that can be used to simulate the results. Both the experiments and the simulations reproduce the picosecond relaxation times, as well as the broadband, tunable nature of this method. Further, the modulation occurs at the time of coupling, allowing for highly modulated signals without the energy losses associated with the propagation of SPP. Indeed, we demonstrate that modulations of the efficiency of a grating coupler by 40–60 % are possible, an order of magnitude improvement over previous results.

We examine the balances associated with this approach. We show that the sign of the modulation is determined by the excitation geometry, and we demonstrate that it is possible to achieve temporally separated modulations of opposite signs at individual wavelengths. Though there is a tradeoff between the total coupling efficiency and the maximum achievable modulation, we suggest that this can be overcome by using custom gratings with sharper SPP resonances.

Although this demonstration is based on the properties of gold, this method should be equally applicable to other metals, if at differing wavelengths as determined by their band structures. It is this very versatility of this method and wide array of different results that are achievable by a careful selection of the system parameters that make it a significant step toward the realization of a plasmonic-based device that is compatible with information and communication applications.

ACKNOWLEDGMENTS

We gratefully thank Markus Betz for comments and insights. We are indebted to Michael G. Helander and Zheng Hong Lu for their assistance with sample fabrication and characterization. We acknowledge funding provided by the Natural Sciences and Engineering Research Council of Canada.

*nrotenbe@physics.utoronto.ca

[1] W. L. Barnes, A. Dereux, and T. W. Ebbesen, Nature (London) **424**, 824 (2003).
[2] E. Ozbay, Science **311**, 189 (2006).
[3] E. Hendry, M. J. Lockyear, J. Gómez Rivas, L. Kuipers, and M. Bonn, Phys. Rev. B **75**, 235305 (2007).
[4] A. K. Azad, H.-T. Chen, S. R. Kasarla, A. J. Taylor, Z. Tian, X. Lu, W. Zhang, H. Lu, A. C. Gossard, and J. F. O'Hara, Appl. Phys. Lett. **95**, 011105 (2009).
[5] K. F. MacDonald, A. V. Krasavin, and N. I. Zheludev, Opt. Commun. **278**, 207 (2007).
[6] R. A. Pala, K. T. Shimizu, N. A. Melosh, and M. L. Brongersma, Nano Lett. **8**, 1506 (2008).
[7] N. Rotenberg, M. Betz, and H. M. van Driel, Opt. Lett. **33**, 2137 (2008).
[8] K. F. MacDonald, Z. L. Sámson, M. I. Stockman, and N. I. Zheludev, Nat. Photonics **3**, 55 (2008).
[9] R. Rosei, F. Antonangeli, and U. M. Grassano, Surf. Sci. **37**, 689 (1973).
[10] S. I. Anisimov, B. L. Kapeliovich, and T. L. Perel'man, Zh. Eksp. Teor. Fiz. **66**, 776 (1974) [Sov. Phys. JETP **39**, 375 (1974)].
[11] C.-K. Sun, F. Vallée, L. H. Acioli, E. P. Ippen, and J. G. Fujimoto, Phys. Rev. B **50**, 15337 (1994).
[12] R. H. M. Groeneveld, R. Sprik, and A. Lagendijk, Phys. Rev. B **51**, 11433 (1995).
[13] N. Rotenberg, A. D. Bristow, M. Pfeiffer, M. Betz, and H. M. van Driel, Phys. Rev. B **75**, 155426 (2007).
[14] H. Raether, in *Surface Plasmons*, edited by G. Hohler (Springer, Berlin, 1988).
[15] Z. Lin and L. V. Zhigilei, Proc. SPIE **6261**, 62610U (2006).
[16] J. Hohlfeld, S.-S. Wellershoff, J. Güdde, U. Conrad, V. Jähnke, and E. Matthias, Chem. Phys. **251**, 237 (2000).
[17] J. Krüger and W. Kautek, Adv. Polym. Sci. **168**, 247 (2004).
[18] L. Li, J. Chandezon, G. Granet, and J.-P. Plumey, Appl. Opt. **38**, 304 (1999).
[19] P. B. Johnson and R. W. Christy, Phys. Rev. B **6**, 4370 (1972).